Predictive capabilities of 2D and 3D block propagation models integrating block shape assessed from field experiments

Franck Bourrier, Vincent Acary

Predictive capabilities of 2D and 3D block propagation models integrating block shape assessed from field experiments

F. Bourrier[a,b] and V. Acary[b]

ARTICLE HISTORY
Compiled March 1, 2021

Abstract

Block propagation models have been used for years for rockfall hazard assessment. However, the settings of model parameters that guarantee the predictive capabilities of the simulations for a given study site remains a key issue.

This research aims at investigating the predictive capabilities of block propagation models after a preliminary calibration phase. It is focused on models integrating the shape of blocks since, despite their sound physical bases, they remain less used than lumped-mass approaches due to their more recent popularisation.

Benefiting from both a recently built model integrating block shape usable in 2D and 3D and from recent experimental results at the slope scale, we first performed an expert-based calibration based on the use of the 2D model and, second, evaluated the predictive capabilities of the calibrated model in 2D and in 3D using the remaining part of the experimental results.

The calibrated model simulations predict the main characteristics of the propagation. Similar level of adequacy between simulations and experimental results in the calibration and validation phases emphasizes genericity of the model settings which guarantees practical applicability : after a calibration phase on sufficient amount of soil types, the model may be used in a predictive manner. The adequacy between 2D and 3D simulations also favors applicability of the model since easier and faster calibrations based on 2D simulations only can be envisaged.

As classically observed for block propagation models, the model is not sufficient to predict the details of the velocity and stopping points but provides accurate prediction of the global ranges of these quantities, in particular of the extreme values. To lift these limitations in terms of predictive capabilities, more advanced calibration procedures based on optimization techniques can constitute a promising perspective.

KEYWORDS
rockfall, model, propagation, fields experiments, calibration

CONTACT F. Bourrier Email: franck.bourrier@inrae.fr

1. Introduction

Block propagation analysis is a key element in the process of rockfall hazard assessment. Although empirical approaches remain used, block propagation is generally quantitatively analysed using process-based models (Volkwein et al., 2011). Among these, classical 2D lumped-mass models are still extensively used. They consider the block as a moving material point that propagates in interaction with the terrain, modelled as a 2D profile. Several levels of complexity exist regarding the modelling of the interaction between the block and the terrain, allowing to account, more or less in details, for the effects of terrain and block properties (Bourrier and Hungr, 2013; Dorren, 2003; Volkwein et al., 2011). Despite the historical preeminence of 2D lumped-mass models, an increase in the use of more complex models has been observed for approximately twenty years. Several 3D lumped-mass models (e.g. Crosta and Agliardi, 2004; Dorren, 2003; Guzzetti et al., 2002; Lan et al., 2007) have been developed and are largely used. Models explicitly integrating block shape (e.g. Descoeudres and Zimmermann, 1987; Koo and Chern, 1998; Leine et al., 2014; Toe et al., 2018) have been more recently applied for practical case studies. Such models exist for long (Descoeudres and Zimmermann, 1987; Falcetta, J.L., 1985) but their practical use was favored by the recent increase in computational capabilities. The relatively recent interest in these models entails that the research results related to them (e.g. Garcia et al., 2020; Lu et al., 2019, 2020; Toe et al., 2018; Yan et al., 2020) are substantially less profuse than those related to lumped-mass models, in particular concerning their calibration and use in practice.

Although block propagation models have been used for years, the settings of the model parameters to guarantee the predictive capabilities of the simulations for a given study site remains difficult. As the number of existing rockfall events on the site of interest is usually very small, even sometimes nil, this settings cannot only be based on the comparison to these events. Most of practitioners favor settings based on the use of typical ranges of parameters values depending on the soil type, obtained from back analysis of simulations on several sites or given by the model developers. These values may be adjusted depending on the experience of the practitioner and on the observed deposited blocks and previous events on the site. Generally, the predictive capabilities of the simulations cannot directly be assessed, because of limited events in the site. Consequently, it relies on the quality of the block propagation model and of the associated calibration.

The calibration process complexity mainly depends on the characteristics of the propagation model. The use of models based on sound physical approaches simplifies the calibration process since such models are generally robust and involve parameters with clear physical meanings. The number of model parameters should also remain limited to its minimum because the assessment of the relative influence of the parameters is simplified and because it reduces the amount of data required for calibration.

The questions of the amount of data required for a correct calibration and of the type of data required remain open. As mentioned above, the quantity of experimental data required for the calibration highly depends on the robustness of the model and on the number of parameters. Both data at the rebound scale (Asteriou and Tsiambaos, 2018; Bourrier et al., 2012; Labiouse and Heidenreich, 2009; Lu et al., 2019) and at the slope scale (Caviezel et al., 2019; Dorren et al., 2006; Giani et al., 2004; Hu et al., 2017; Spadari et al., 2012; Volkwein et al., 2018; Williams et al., 2020) may be used. Finally, the calibration procedure should remain practically feasible. This question is crucial, especially for models that require large computational efforts, such as the propagation models explicitly integrating block shape.

The objective of this research is to investigate the predictive capabilities of block propagation models integrating the shape of blocks after a preliminary calibration phase, designed to remain practically feasible. In this research work, we benefited from both a recently built model integrating block shape usable both in 2D and 3D and from recent experimental results at the slope scale.

The contributions of the article are as follows. The propagation model used is based on nonsmooth mechanics (Brogliato, 2016; Moreau, 1988), following recent research results in the field (Leine et al., 2014). The nonsmooth approach is a sound modelling framework to obtain a robust numerical method, which satisfies the threshold phenomena (friction, contact) and the dissipation properties of the model in discrete time, in particular impact dissipation and energy properties (Acary, 2015). In this article, the originality is to include rolling friction in addition to more standard phenomena such as frictional, plastic and impact dissipation processes at the interface between the soil and the block. The efficiency of the introduction of the rolling resistance to accurately model the interaction was already shown in (Bourrier et al., 2012; Garcia et al., 2020). The experimental dataset, used in this article is made of data on two propagation paths with similar soil types. It provides sufficiently exhaustive, diversified, and detailed data for a) calibrating the model on the first path, and b) assessing its predictive capabilities on the second one. In addition, the extensive data related with block properties and trajectories on both sites, and the large number of block released, constitutes a substantial advantage for both the calibration and the assessment of predictive capabilities. For the purpose of the study, we built an original, and practically oriented, calibration procedure. We first performed an expert-based calibration based on the use of the 2D model and of part of the results obtained in the field experiments. Second, we evaluated the predictive capabilities of the calibrated model in 2D and in 3D using the remaining part of the experimental results.

The field experiments and the modelling approach are respectively presented in Section 2 and Section 3. The results obtained are then detailed in Section 4, focusing first on the calibration of the model (Section 4.1) and, then, analysing the relevance and robustness of the simulation results (Section 4.2) as well as the predictive capabilities of the model (Section 4.3). Section 5 concludes the article with a detailed discussion

of the results.

2. Field experiments

The field experiments used in this study for the calibration of the model and assessment of its predictive capabilities had been collected with the objective of providing experimental data of block propagation for the assessment of models relevance on configurations where propagation simulations are potentially problematic (Bourrier et al., 2020).

The experiments, carried out in a quarry (Authume, France, owner: Pernot S.A), consisted in the successive release of more than one hundred blocks on two propagation paths. The first path, referred to as path A (Fig. 1), is characterized by an upper gentle slope section, made of newly deposited quarry waste, mixing sand, clay, and limestone fragments. This upper slope is overhanging a subvertical rock cut made of compact limestone rock and, at the toe of this wall, an horizontal track, made of compact quarry waste. A second rock cut, with same characteristics as the first one, separates this track from the quasihorizontal platform, also made of compact quarry waste, acting as terminal deposit area. The second path, referred to as path B (Fig. 2), is characterized, in its upper section, by an inclined slope made of medium soft quarry waste, mixing sand, clay, and limestone fragments. This slope is bordered, at mid-distance, by a rock cut on one side and by a talus on the other, which creates a so-called corridor. The intermediate section of path B is characterized by two successive tracks, made of compact quarry waste, and separated by a short slope, made of medium soft quarry waste. The second track is followed by an inclined slope also made of medium soft quarry waste, terminated by a globally horizontal deposit area, made of compact quarry waste. For both paths, the altitude difference between the top and the bottom of the path is approximately $45m$.

A Digital Terrain Model (DTM - resolution: $0.2m$) was built in order to perform analyses of block trajectories. The DTM was generated from a set of images, taken from a UAV and from the ground. The images were treated using photogrammetry techniques (software Agisoft V1.2.6). A set of 20 control points covering the site, and located in a local coordinate system using a theodolite (Leica TS02), was used in the building process. Two GPS points and one geodesic point were also recorded to georeference the DTM.

Approximately fifty blocks were successively released on each propagation path using a power shovel. A release zone ($4m$ x $4m$ horizontal area) was delimited at the top of each path. The vertical release heights were set at $4m$ for path A and $2m$ for path B.

The blocks used in the experimental campaign were visually selected to obtain block volumes approximately ranging between 0.1 and $0.75m^3$. Each block was weighted and three principal lengths (L_1, L_2, and L_3, with $L_1 > L_2 > L_3$) have been measured for

each block. These lengths characterize the minimal parallelepiped that incorporates the block.

The quantitative analysis of block kinematics focused on measurements at specific locations of the site, called *Evaluation Screens (ES)* (Figures 1 and 2), using cameras with shooting range focused on the *ES*. For path A, the first evaluation screen ($ES1-A$) was located at the end of the uphill gentle slope, just before the first rock cut, and the second one ($ES2-A$) at the top of the downhill rock cut. For path B, $ES1-B$ is the contour line at the elevation of the corridor beginning while $ES2-B$ was located at the downstream extremity of the first sloping track.

The blocks velocities were measured at the *ES*. For these measurements, two locations of the block before and after the ES and the duration taken by the block to travel this distance were first measured from projections of the video footage images on the DTM of the site. Second, the velocity at the ES was calculated assuming either free flight or rolling of the block. The error in terms of velocity measurement is mainly due to errors on the visual positioning of the points on the DTM. This error is estimated around $0.5m$, inducing errors on the velocity around $1m/s$.

Complementary, precise determination of the blocks stopping points locations was conducted after each series of five blocks release. The theodolite used for this purpose (Leica TS02) provided measurements with an estimated accuracy of $0.1m$, mainly resulting from uncertainties associated with the visual assessment of blocks gravity centers. In case of breakage of the block, the stopping point considered was the stopping point of the larger resulting fragment, if it could be identified, or the last impact point before breakage, if the block broke in several small pieces.

Details about the study site, the experimental protocol, and the measurements can be found in (Bourrier et al., 2020).

As the experimental dataset is made of data on two propagation paths with similar soil types, it is very well adapted for, first, calibrating a propagation model on one path And, second, assessing the predictive capabilities of the model on the second one. In addition, the number of different types of soils remains limited (medium compacted quarry wastes, compacted quarry wastes, and compact rock), which simplifies the calibration phase, and the type of soils are similar on both paths, which is crucial for a calibration on one path, followed by an assessment of predictive capabilities on the second one. Finally, the extensive data related with block properties and trajectories on both sites and the large number of block released constitutes a substantial advantage for both the calibration and the assessment of predictive capabilities.

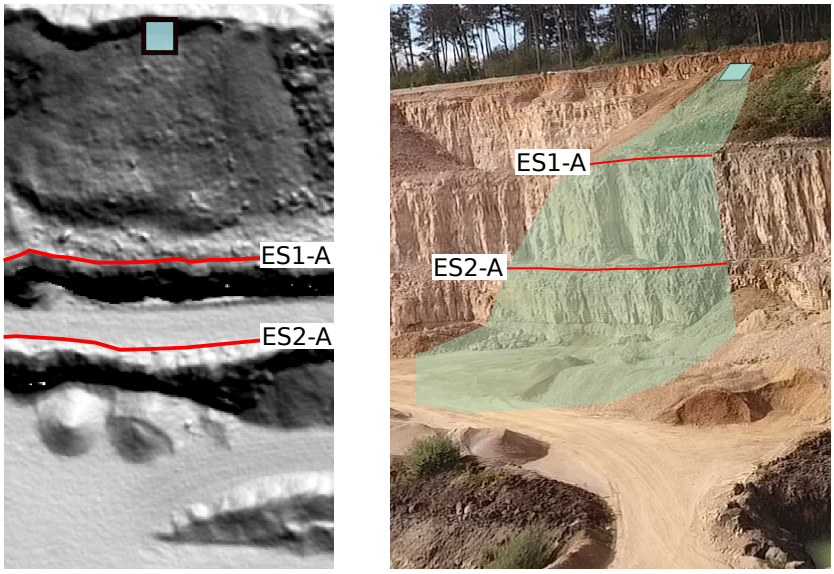

Figure 1.: Overview of path A (a : topview of a hillshade built from a 1m resolution DTM, b : general view) including the location of the Evaluation Screens ($ES1-A$ and $ES2-A$), of the release zone (green squared zone), and of the potential propagation zone (light green zone).

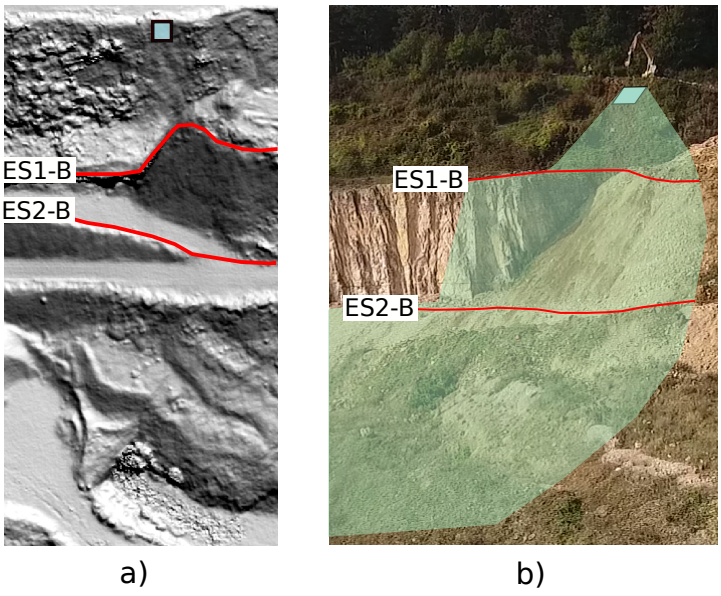

Figure 2.: Overview of path B (a : topview of a hillshade built from a 1m resolution DTM, b : general view) including the location of the Evaluation Screens ($ES1-B$ and $ES2-B$), of the release zone (green squared zone), and of the potential propagation zone (light green zone).

3. Block propagation modelling

3.1. Propagation model description

The propagation model was developed using the Siconos software (Acary et al., 2019)[1]. Siconos is an open-source scientific software primarily targeted at modeling and simulating nonsmooth dynamical systems.

The propagation model allows to simulate the 3D propagation of a block modelled as a convex facetized rigid body interacting with a terrain, modelled as a triangulated surface. In 2D, the block is a polygon, and the surface a polyline. As classically done in block propagation models, successive releases of blocks with different initial conditions are simulated to quantify the variability of the block propagation process. For each block, the propagation modelling is a time-stepping process. At each time step, the occurrence of an interaction between the block and the surface is checked. In the case of an interaction, an impulse is applied to the block. The propagation stops when the block reaches its static equilibrium.

3.1.1. Propagation of a block

In a three-dimensional configuration, the position of the block center of mass is denoted $x_{\mathsf{g}} \in I\!R^3$, and the block orientation is characterized by a the rotation matrix $\mathbf{R} \in I\!R^{3\times 3}$ of the body-fixed frame with respect to a given inertial frame. The rotation matrix is parametrized by a unit quaternion $\mathsf{q} \in I\!R^4$, $\|\mathsf{q}\| = 1$ such that $\mathbf{R} = \Phi(\mathsf{q})$, $\dot{\mathsf{q}} = \Psi(\mathsf{q})\Omega$ where $\Omega \in I\!R^3$ is the angular velocity of the body expressed in the body–fixed frame. Formulae for Φ and Ψ can be found in standard textbooks on multi-body dynamics (Géradin and Cardona, 2001). We denote by q the generalized coordinates vector of the block, and by v the associated generalized velocities vector:

$$q \coloneqq \begin{bmatrix} x_{\mathsf{g}} \\ \mathsf{q} \end{bmatrix}, \quad v \coloneqq \begin{bmatrix} v_{\mathsf{g}} \\ \Omega \end{bmatrix}. \tag{1}$$

The relation between v and the time derivative of q is

$$\dot{q} = \begin{bmatrix} \dot{x}_{\mathsf{g}} \\ \Psi(\mathsf{q})\dot{\mathsf{q}} \end{bmatrix} = \begin{bmatrix} I_3 & 0 \\ 0 & \Psi(\mathsf{q}) \end{bmatrix} v \coloneqq T(q)v \tag{2}$$

with $T(q) \in I\!R^{7\times 6}$, and I_3 the identity matrix. Note that the generalized velocities vector v is not directly the time derivative of the generalized coordinates vector.

[1] http://github.com/siconos/siconos

The Newton-Euler equation in compact form may be written as:

$$\begin{cases} \dot{q} = T(q)v, \\ M\dot{v} = F(q,v) \end{cases} \tag{3}$$

$M \in I\!R^{6\times 6}$ is the total inertia matrix

$$M := \begin{pmatrix} mI_3 & 0 \\ 0 & I \end{pmatrix}, \tag{4}$$

where $m > 0$ is the mass, $I \in I\!R^{3\times 3}$ is the matrix of moments of inertia around the center of mass and the axis of the body–fixed frame. The explicit dependence on time of functions is not mentioned.

The vector $F(q,v) \in I\!R^6$ collects all the forces and torques applied to the body

$$F(q,v) := \begin{pmatrix} f(x_{\mathsf{g}}, v_{\mathsf{g}}, \mathsf{q}, \Omega) \\ I\Omega \times \Omega + t(x_{\mathsf{g}}, v_{\mathsf{g}}, \mathsf{q}, \Omega) \end{pmatrix}. \tag{5}$$

where the vectors $f(\cdot) \in I\!R^3$ and $t(\cdot) \in I\!R^3$ are the total forces and torques applied to the body. The term $I\Omega \times \Omega$ stands for the gyroscopic forces.

Among the other forces and torques applied to the body, those induced by the contact between the slope surface and the block are essential. In the model, these forces are considered as unilateral constraints applied to the block. The distance between the block and the surface is associated with a gap function $g(q)$ and the block is subjected to the unilateral constraint $g(q) \geq 0$, that prevents from the penetration of the block into the ground. The unilateral constraint generates a generalized reaction force applied to the body defined by $R \in I\!R^6$.

The value of R is characterized using an impact law that governs the interaction between the block and the slope surface. Impact laws are classically expressed in local contact frames. For that reason, the local relative velocity u and the local reaction p are expressed in terms of generalized variables with linear relations for a given q as:

$$\begin{aligned} u &= G^\top(q)v \\ R &= G(q)p. \end{aligned} \tag{6}$$

where $G^\top(q)$ is the operator relating local variables to global ones.

In the simple case of m frictionless unilateral constraints, the Newton-Euler equa-

tions can thus be written as :

$$\begin{cases} \dot{q} = T(q)v, \\ M\dot{v} = F(q,v) + R \\ u = G^\top(q)v, \quad R = G(q)p \\ 0 \ \leq \ g(q) \perp p \ \geq \ 0. \end{cases} \tag{7}$$

where $u \in I\!R^m, p \in I\!R^m$ and $G(q) \in I\!R^{6\times m}$. The inequalities involving vectors are understood to hold component-wise and the $x \perp y$ symbol means that $y^\top x = 0$. The last line of (7) is the contact law, also known as the Signorini condition.

A specific impact law involving Coulomb friction with rolling resistance at the contact was implemented in the model. This law involves a standard Coulomb friction law which is a set-valued force law that generates a resistive force to sliding, *i.e.* opposite to the sliding velocity. The standard rolling friction law, considered in this article, is also a set-valued force law that generates a resistive moment to rolling, *i.e.* opposite to the rolling velocity. This rolling friction model has been developed in (Acary and Bourrier, 2021) and only the main features are recalled in a three-dimensional setting, but the following formulation can be easily specified for a 2D configuration.

As mentioned previously, the formulation of the impact law requires the definition of local variables at contact. Let assume that we can uniquely define an orthonormal contact frame at the contact point C denoted by $(C, \mathsf{N}, \mathsf{T_1}, \mathsf{T_2})$, where $\mathsf{N} \in I\!R^3$ defines an outward unit normal vector to the block at point C and $\mathsf{T_1} \in I\!R^3, \mathsf{T_2} \in I\!R^3$ are unit tangent vectors. The reaction force exerted by the block on the surface is denoted by $r \in I\!R^3$. It can be decomposed in the contact frame as

$$r \coloneqq r_{\mathrm{N}}\mathsf{N} + r_{\mathrm{T}_1}\mathsf{T_1} + r_{\mathrm{T}_2}\mathsf{T_2}, \qquad \text{with } r_{\mathrm{N}} \in I\!R \text{ and } r_{\mathrm{T}} \coloneqq [r_{\mathrm{T}_1}, r_{\mathrm{T}_2}]^\top \in I\!R^2, \tag{8}$$

where r_{T} is the tangent reaction, that will be used to model Coulomb friction. The relative velocity at contact $u \in I\!R^3$ is used as natural way to formulate friction. It is also decomposed as

$$u \coloneqq u_{\mathrm{N}}\mathsf{N} + u_{\mathrm{T}_1}\mathsf{T_1} + u_{\mathrm{T}_2}\mathsf{T_2} \quad \text{with } u_{\mathrm{N}} \in I\!R \text{ and } u_{\mathrm{T}} = [u_{\mathrm{T}_1}, u_{\mathrm{T}_2}]^\top \in I\!R^2, \tag{9}$$

where u_{T} is the sliding relative local velocity. In order to formulate the rolling friction at contact, we also introduce the relative angular velocity $\omega_{\mathrm{R}} \in I\!R^2$ and the rolling friction reaction torque $m_{\mathrm{R}} \in I\!R^2$ at contact. To obtain a compact formulation of the impact model, we denote the local variables at contact by:

$$p \coloneqq \begin{bmatrix} r_{\mathrm{N}} \\ r_{\mathrm{T}} \\ m_{\mathrm{R}} \end{bmatrix} = \begin{bmatrix} r \\ m_{\mathrm{R}} \end{bmatrix} \text{ and } y \coloneqq \begin{bmatrix} u_{\mathrm{N}} \\ u_{\mathrm{T}} \\ \omega_{\mathrm{R}} \end{bmatrix} = \begin{bmatrix} u \\ \omega_{\mathrm{R}} \end{bmatrix}. \tag{10}$$

At the velocity level, the Signorini condition is written

$$\begin{cases} 0 \leq u_{\mathrm{N}} \perp r_{\mathrm{N}} \geq 0 & \text{if } g(q) \leq 0 \\ r_{\mathrm{N}} = 0 & \text{otherwise.} \end{cases} \tag{11}$$

The motion of the block is expected to be nonsmooth since impacts occur when the block hits the ground. The model must be completed by an impact law that will define the post-impact velocity u_{N}^{+} with respect to, at least, the pre-impact velocity u_{N}^{-}. The simplest choice is to use the Newton impact law that can be written as

$$u_{\mathrm{N}}^{+} = -e_c u_{\mathrm{N}}^{-}, \tag{12}$$

where $e_c \geq 0$ is the coefficient of restitution. If impact occurs, the reaction p, and its components, r and m_{R} are no longer homogeneous to forces but to impulses. As it is usually done in impact mechanics (Brogliato, 2016; Moreau, 1988), the contact law with unilateral constraints and friction is written in terms of local relative velocities and impulses. The Newton impact law can be included in the complementary condition at the velocity level as

$$0 \leq \bar{u}_{\mathrm{N}} \perp r_{\mathrm{N}} \geq 0 \text{ if } g(q) \leq 0, \tag{13}$$

with $\bar{u}_{\mathrm{N}} \coloneqq u_{\mathrm{N}}^{+} + e_c u_{\mathrm{N}}^{-}$ and r_{N} is the normal reaction impulse. For $g(q) > 0$, we trivially have $p = 0$. For $g(q) \leq 0$, the Coulomb friction model with unilateral contact and rolling resistance is defined in all modes, following the work in (Acary and Bourrier, 2021) :

- take–off

$$p = 0, \bar{u}_{\mathrm{N}} \geq 0, \tag{14}$$

- sticking and no-rolling

$$p \in K_r, u = 0, \omega_{\mathrm{R}} = 0, \tag{15}$$

- sliding and no-rolling

$$p \in K_r, \bar{u}_{\mathrm{N}} = 0, \|r_{\mathrm{T}}\| = \mu_c r_{\mathrm{N}}, \|m_{\mathrm{R}}\| < \mu_{r,c} r_{\mathrm{N}}, \|r_{\mathrm{T}}\| u_{\mathrm{T}} = -\|u_{\mathrm{T}}\| r_{\mathrm{T}}, \omega_{\mathrm{R}} = 0, \tag{16}$$

- sticking and rolling

$$p \in K_r, \bar{u}_{\mathrm{N}} = 0, \|r_{\mathrm{T}}\| < \mu_c r_{\mathrm{N}}, \|m_{\mathrm{R}}\| = \mu_{r,c} r_{\mathrm{N}}, \|m_{\mathrm{R}}\| \omega_{\mathrm{R}} = -\|\omega_{\mathrm{R}}\| m_{\mathrm{R}}, u_{\mathrm{T}} = 0, \tag{17}$$

- and sliding and rolling

$$\begin{aligned} p \in \partial K_r, \bar{u}_{\mathrm{N}} = 0, \|r_{\mathrm{T}}\| = \mu_c r_{\mathrm{N}}, \|m_{\mathrm{R}}\| = \mu_{r,c} r_{\mathrm{N}}, \\ \|r_{\mathrm{T}}\| u_{\mathrm{T}} = -\|u_{\mathrm{T}}\| r_{\mathrm{T}}, \quad \|m_{\mathrm{R}}\| \omega_{\mathrm{R}} = -\|\omega_{\mathrm{R}}\| m_{\mathrm{R}}, \end{aligned} \tag{18}$$

where the extended friction cone K_r is defined as the cone of admissible reaction forces and torques, by

$$K_r = \{p \in I\!R^5 \mid \|r_{\mathrm{T}}\| \leq \mu r_{\mathrm{N}}, \quad \|m_{\mathrm{R}}\| \leq \mu_{r,c} r_{\mathrm{N}}\} \subset I\!R^5, \tag{19}$$

and its boundary is given by

$$\partial K_r = \{p \in I\!R^5 \mid \|r_{\mathrm{T}}\| = \mu r_{\mathrm{N}}, \quad \|m_{\mathrm{R}}\| = \mu_{r,c} r_{\mathrm{N}}\} \subset I\!R^5. \tag{20}$$

Although the model of the interaction between the block and the soil does not allow explicitly accounting for soil deformation during impact, it integrates block energy losses due to plasticity, viscosity and wave propagation by means of the restitution coefficient e_c. The frictional processes at the interface are also accounted for using μ_c. Finally, the rolling friction coefficient $\mu_{r,c}$ quantifies cratering and resistance of the soil to block rolling around the contact point.

Some details on the numerical implementation of the complete rolling friction model can be found in (Acary and Bourrier, 2021). In this work, the simulations have been done with the Moreau–Jean time–stepping scheme (Acary and Brogliato, 2008; Jean and Moreau, 1987) based on a θ-method for the smooth terms and the projected Gauss-Seidel for the discrete frictional contact problems (Acary et al., 2018; Jourdan et al., 1998). The numerical methods are implemented in the Siconos software (freely available as a free open-source software) and the version v4.3.0 is used in this article.

The θ parameter is set equal to $1/2$ to avoid the numerical dissipation of energy due to the time-stepping scheme (Acary, 2015). The time step and the error of the projected Gauss-Seidel solver are set at $10^{-3}s$ and 10^{-4}, respectively. Under these simulation conditions, the computational effort to compute the propagation of 50 blocks on path A or B is typically of few minutes for 2D simulations and few hours for 3D ones on a personal laptop, provided that the numerical model is not optimized.

3.1.2. Simulation of the blocks propagation

In total, the simulation of blocks propagation requires the definition of the terrain, as a triangulated surface or a polyline, of the block geometry, as a meshed polyhedron or polygon, of the soil properties in all points of the site, by means of three parameters (e_c , μ_c, $\mu_{r,c}$), and of the initial release conditions (block location and orientation).

The block size, global shape (characterized by the three dimensions of the minimal parallelepiped including the block), and initial release conditions (initial location and

orientation) can be either defined **a)** as single values, if a specific unstable rock compartment is identified, or **b)** as variables quantities, if different block sizes, shapes and initial release conditions, have been identified in a field survey.

Global homogeneous zones in the site are defined and associated with different soil properties, i.e. with deterministic values of e_c , μ_c, $\mu_{r,c}$. Indeed, we assume that the variability of the soil properties in a homogeneous zone is a minor cause of block trajectories variability.

Finally, the detailed block shape and initial orientation are randomly set for each block release, assuming that these quantities are the main causes of the variability of the block propagation process.

3.2. Simulations of the experiments

For the 3D simulations of the experiments, a $1m$ resolution DTM was built from the resampling of the $0.2m$ resolution DTM generated. The decrease in DTM resolution is mandatory because, as the model of the interaction between the block and the soil does not explicitly integrates soil plastic strains, a $0.2m$ resolution DTM would model local topography details that are suppressed in real impacts due to cratering. One can note that the decrease in DTM resolution also decreases drastically computational durations.

Profiles starting from the release zones were extracted from the $1m$ DTM for the 2D simulations. The profiles were chosen from expert assessment of the main propagation corridors. For path A, the profile was generated along the steepest slope direction. For path B, a profile passing through the upper corridor, bordered by a rock cut and a talus, and following the steepest slope direction down this corridor was built. At the crossing with the tracks, the profile crosses the track following the steepest slope direction of the above slope.

Each block propagation simulation set corresponds to the simulation of n block propagations. For each propagation simulation set, the stopping points of all blocks were stored as well as the velocities and heights of the blocks passing through the ES.

For each block propagation, a set of four block properties (three block dimensions L_1, L_2, L_3, and the block mass m_b) was sampled among the quantities measured in the experiments. A convex polyhedron in 3D, or a convex polygon in 2D, was generated so as to fit into a parallepiped of dimensions L_1, L_2, L_3 in 3D, or a rectangle of dimensions L_1, L_2 in 2D. The polyhedron, or polygon, generation procedure consists in generating a point cloud, then identifying the points bordering the point cloud and, finally, creating a convex envelope using these points (triangulated surface in 3D or polyline in 2D). The number of points of the initial point cloud impacts the shape of the polyhedron or polygon (see section 4.2). Finally, the mass of the measured block was affected to the body generated.

The horizontal initial coordinates of the blocks were randomly chosen within ranges

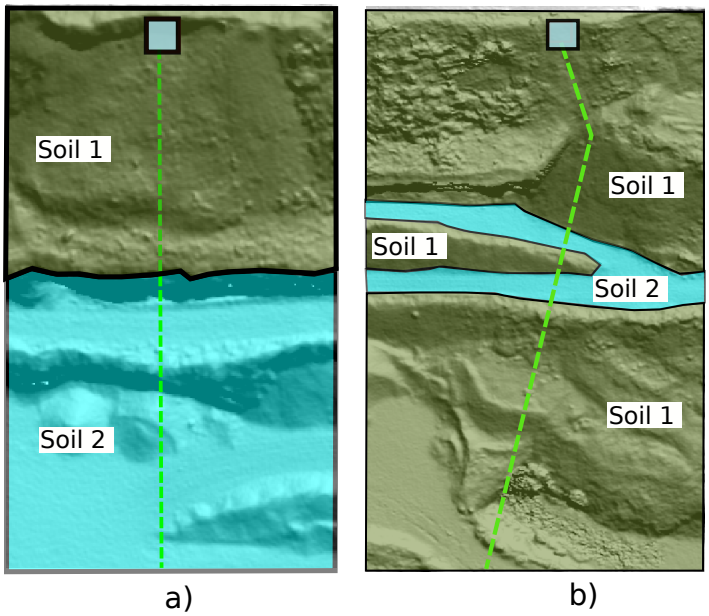

Figure 3.: Homogeneous zones in terms of soil properties determined by expert knowledge on the propagation paths A (a) and B (b). Two different soil types were defined in the site.

of values corresponding to the experiments. The initial vertical location of the block was defined so that the initial height of the block gravity centre above the slope surface was equal to $4m$ for path A, or $2m$ for path B. Finally, the orientation was randomly set using one random unit quaternion in 3D or one random angle in 2D.

Homogeneous zones in terms of soil properties (Fig. 3) were determined by expert knowledge with the objective of limiting the different types of soils. Assuming that the subvertical rock cuts are not impacted by blocks, only two different soil types were defined in the site: loose quarry waste, mixing sand, clay, limestone fragments, encountered in slope zones, and compact quarry waste, corresponding to the tracks and terminal deposit areas. Fixed values of the three parameters associated with soil properties were set for each soil type.

Finally, for each simulation set (Fig. 4), the only physical unknown parameters are the soil properties that are set to match the results (calibration phase) or according to previous results (validation phase).

4. Calibration and assessment of the block propagation model

The originality of the approach proposed in this research work lies in the design of an original calibration procedure. In this procedure, the calibration is based on 2D propagation models, which favors its feasibility given the computational efficiency of 2D models. In addition, the experimental dataset allows to separate the calibration of

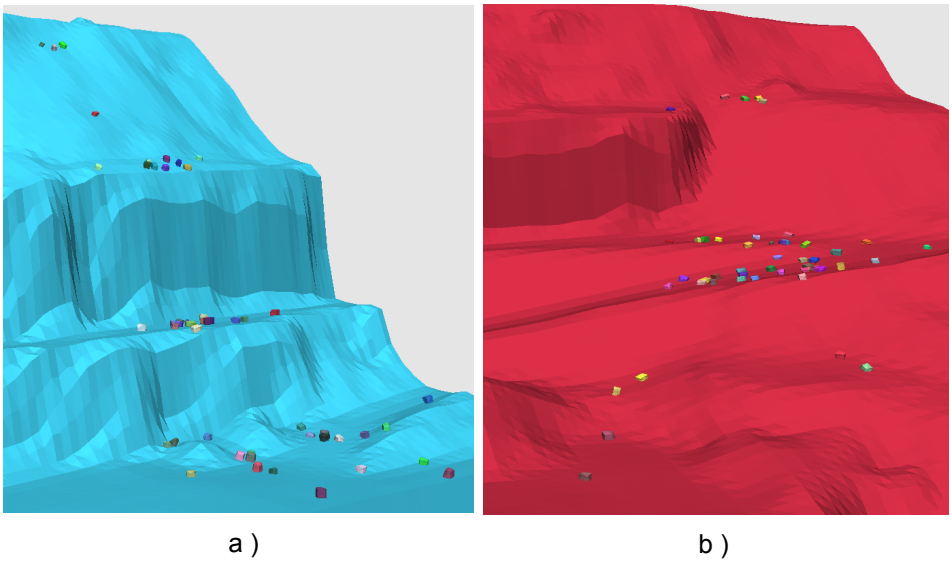

Figure 4.: Examples of block stopping points obtained from propagation simulations on path A (a) and path B (b).

the model and the assessment of its predictive capabilities. Finally, the use of calibration data at the field scale, of block stopping points locations in particular, favors the applicability of the procedure proposed since the latter data is more easily accessible to practitioners, compared to data at the rebound scale, in particular.

The calibration phase consists in determining the soil properties associated with the two soil types of the site using 2D simulations. In this phase, only the experimental data on path A were used so that the experimental results obtained for path B could be dedicated to validation only.

The experimental results available for path A correspond to the propagation of fifty blocks along the path. Although rather large, this sample may not be sufficient to assess the complete variability of the block propagation. Substantially different results may have been obtained for another sample. As it is not possible to check this assumption from the experimental results, we choose to perform calibration using simulation sets sets of $n = 50$ block releases in order to compare samples of the same size as in the experiments and to limit the simulation duration. We will assess the relevance of the results obtained by comparing different simulation results obtained with $n = 50$ among each other and with results obtained for increasing numbers of block releases.

We used both the measurements of the stopping points and of the velocities for the comparisons. In 2D, the locations of the stopping points cannot directly be used as the blocks do not necessarily propagate through the profiles chosen for the simulations. Instead of projecting the points on the profile following assumptions subject to caution, we choose to use the percentage of blocks located in experimentally identified preferential deposit zones (Fig. 5).

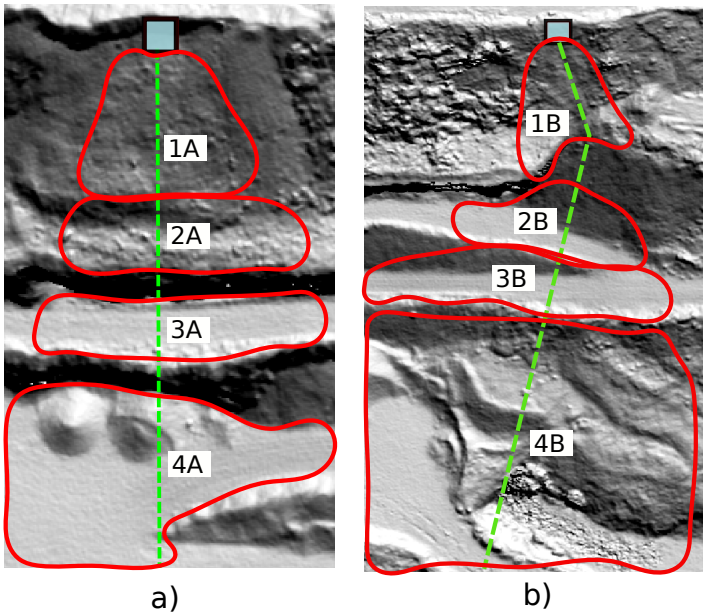

Figure 5.: Preferential deposit zones identified during the experimental campaign for path A (a) and path B (b) (Bourrier et al., 2020).

In the following, the expert-based calibration, that allowed to determine the optimal soil properties, is first presented. Second, the relevance and the robustness of the simulations is analyzed. In particular, the repeatability of the simulation results, the influence of the number n of block propagation per simulation set, of the modelling of the shape of the blocks and of the influence of the soil properties are investigated.

4.1. Expert-based calibration using 2D simulations

The expert-based calibration phase consisted in iteratively selecting the values of the soils properties that lead to the best adequacy between the simulation and the experimental results. Although more complex calibration procedure, based on optimization processes for example (Mollon et al., 2012), could have been more efficient, we choose an expert-based calibration to remain in the context of classical use of block propagation models by practitioners.

The first step of the calibration consisted in setting values of the soils properties for Soil 1 (Fig. 3) that traduce the trajectories of the block along the uphill slope. In this part of the slope, the blocks propagate by successions of very small rebounds which induces low velocities, ranging between almost nil ones and $7.5 m/s$ (Fig. 6), at $ES1 - A$. Few blocks are stopped in this part of the slope : 2% of the blocks are stopped in zone 1A and 2% in zone 2A.

The setting of parameters for Soil 1 is challenging because it requires finding sets of values that allow propagation of the block at low velocity until $ES1-A$ and few blocks

	Soil 1	Soil 2
e_c	0.	0.
μ_c	0.5	0.6
$\mu_{r,c}$ (m)	0.04	0.05

Table 1.: Soils properties obtained from expert-based calibration

stops in zones $1A$ and $2A$. The best fit parameters obtained (Table 1) allow to obtain very few block stops and similar velocity ranges as in the experiments at $ES1-A$ (Fig. 6). However, one can note that the parameters chosen entail slight overestimation of the blocks stopping in zones $1A$ and $2A$ and, even if velocity ranges are similar. Despite these differences, the parameters sets chosen remains the more suitable obtained from expert-based calibration. Other sets of parameters either yielded too many blocks stopped before $ES1-A$ or too large velocities at $ES1-A$.

The direct setting of parameters associated with Soil 2 at the same values as for Soil 1 (Fig. 6 - 1 zone) provides simulation results in adequacy with experimental results in terms of velocities ranges at $ES2-A$ and of relative distribution between the blocks stopped in zones $3A$ and $4A$. The predictions of both quantities were improved (Fig. 6 - 2 zones) considering that Soil 2 leads to more frictional dissipation (Table 1), i.e. larger values of both μ_c and $\mu_{r,c}$, since it is more compact.

One can note that the differences between the two latter simulations for zones $1A$ and $2A$ as well as for $ES1-A$ illustrate the fact that using $n = 50$ is not sufficient for a complete assessment of the variability of the simulation results due to different initial block shapes and orientations.

Finally, in an attempt to improve the predictions of block propagation in the upper part of the slope, a third zone, corresponding to the release zone of the blocks (Fig. 1) was defined. $\mu_{r,c}$ was set at nil value in this zone to favor initial propagation of the blocks (Fig. 6 - 3 zones) which improves the prediction of the distribution of block stopping points.

4.2. Relevance and robustness of the simulations

The comparison between different simulation sets for $n = 50$ (Fig. 7) shows that results are qualitatively similar in terms of relative number of blocks stopped in the different zones and of velocity ranges at $ES1-A$ and $ES2-A$. However, significant quantitative differences between the simulation sets exist both in terms of percentages of blocks stopped in the different zones and velocity distributions at the ES.

For increasing values of n (Fig. 8), the differences between the results tend to decrease both in terms of stopping points and velocities but remain, even between large numbers of block releases ($n = 500$ and $n = 2000$, for example). However, the smaller sample ($n = 50$) is a good indicator of the general trends of the simulations for larger values of n.

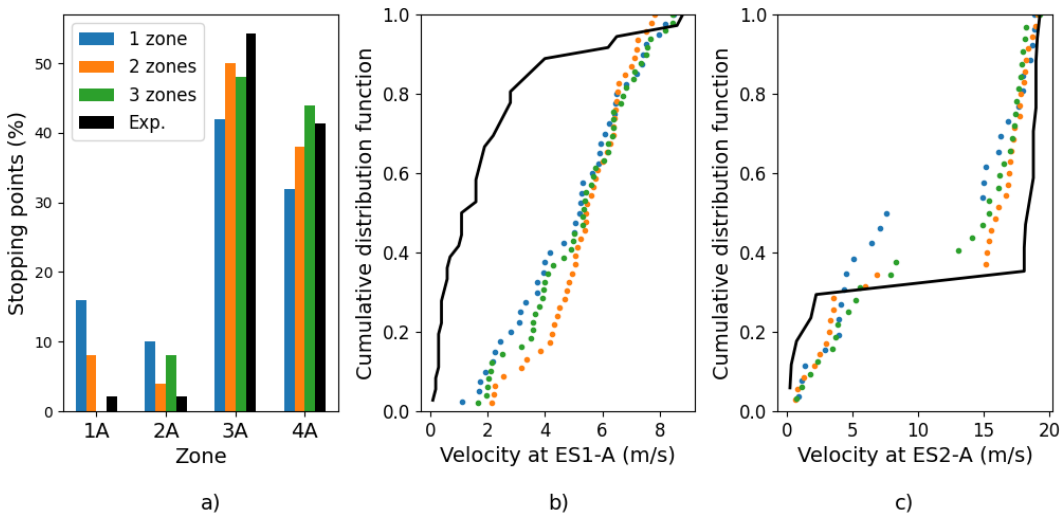

Figure 6.: Comparison between experimental and simulations results obtained for path A using the soil parameters associated with Soil 1 along the complete path (1 zone), or the best fit parameters for Soil 1 and 2 (2 zones), or the best fit parameters for Soil 1 and 2 and $\mu_{r,c} = 0$ in the release zone of the blocks (a : distribution of the stopping points between the preferential deposit zones, b : cumulative distribution function of block velocities at $ES1 - A$, c : cumulative distribution function of block velocities at $ES2 - A$).

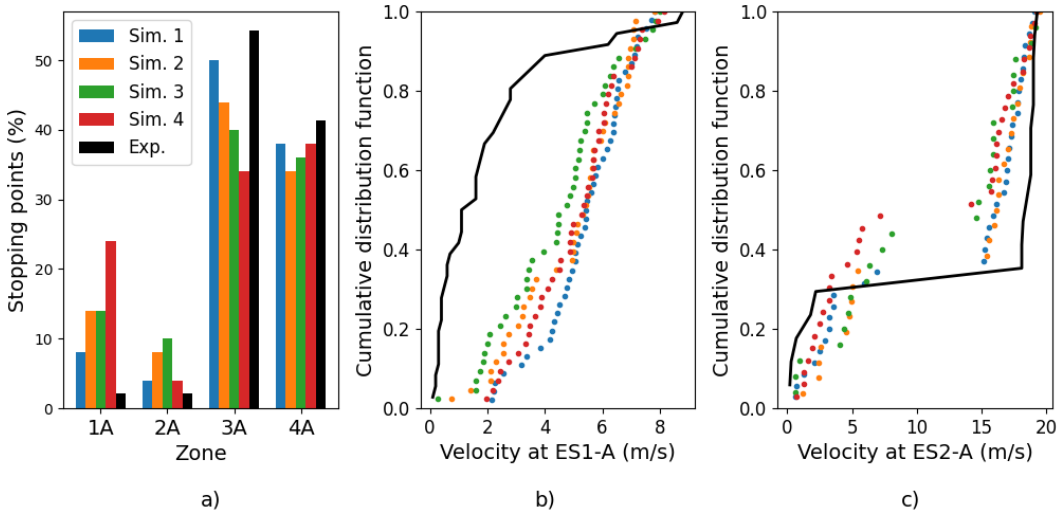

Figure 7.: Results obtained from different simulations of block propagation on path A using the calibrated parameters for soil properties and $n = 50$ (a : distribution of the stopping points between the preferential deposit zones, b : cumulative distribution function of block velocities at $ES1 - A$, c : cumulative distribution function of block velocities at $ES2 - A$).

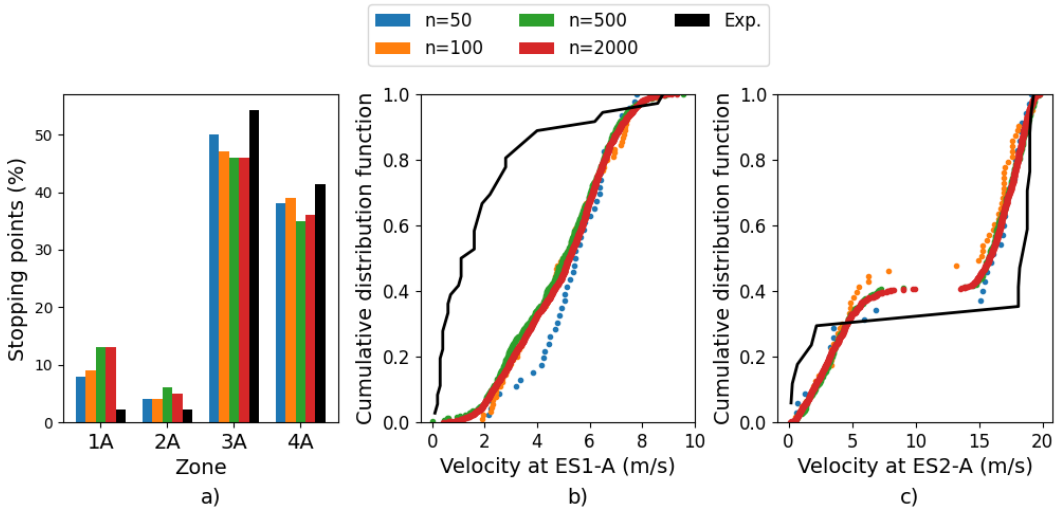

Figure 8.: Results obtained from different simulations of block propagation on path A using the calibrated parameters for soil properties and increasing numbers n of block releases (a : distribution of the stopping points between the preferential deposit zones, b : cumulative distribution function of block velocities at $ES1-A$, c : cumulative distribution function of block velocities at $ES2-A$).

Under the simulation assumptions described in section 3.2, the simulation parameters that can influence the results are the initial orientation, whose influence is explored by making n block releases, the block shape and the soil properties. The influence of the two latter parameters was analysed compared to the variability between the simulation sets for $n = 50$ (Fig. 7).

Simulations with different block shapes have been performed. Rectangular blocks, EOTA (rectangles with "cut corners") blocks (EOTA, 2018), and two convex polygons, made of smaller and larger numbers of segments, were modelled. The shape of the convex polygons was controlled by means of the number of points of the initial point cloud used to generate the convex polygonal envelop: the larger the number of points in the point could, the larger the number of segments of the polygon. These simulations (Fig. 10) showed that the influence of block shape is significantly larger than the variability observed for $n = 50$ (Fig. 7) only for cubes and EOTA blocks. On the contrary, the shape of the random polygons influences in the same order as the variability observed for $n = 50$. The influence of block shape can be explained from a physical point of view. More cubic block shapes entail smaller block propagation distances and velocities.

The influence of soil properties was explored using constant soil properties on the study site. In this analysis, initial values of the soil parameters were first defined. The restitution coefficient e_c was set at nil value, the friction coefficient was set $\mu_c = 0.6$, and the rolling friction coefficient $\mu_{r,c}$ was set at nil value. The influence of each soil parameter was second explored by varying only it. The results obtained show

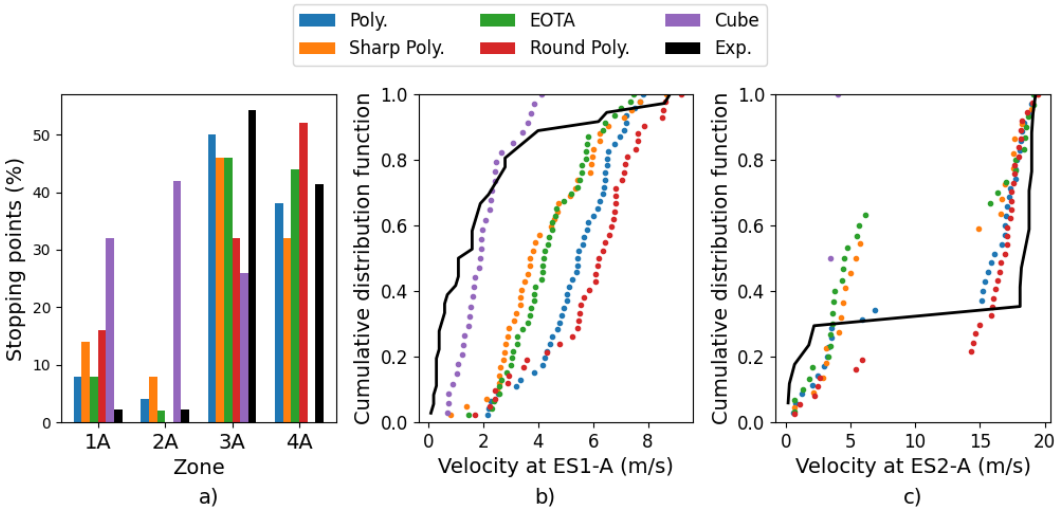

Figure 9.: Results obtained from different simulations of block propagation on path A using the calibrated parameters for soil properties and different block shapes (a : distribution of the stopping points between the preferential deposit zones, b : cumulative distribution function of block velocities at $ES1-A$, c : cumulative distribution function of block velocities at $ES2-A$).

significant influence of e_c (Fig. 11) and $\mu_{r,c}$ (Fig. 12) compared with differences in simulation sets for $n = 50$ (Fig. 7), whereas the influence of μ_c (Fig. 10) remains in the same order of magnitude. As for the influence of block shape, the influence of soil parameters can be explained from a physical point of view. Increase in e_c and decrease in $\mu_{r,c}$ entail less energy dissipation and, consequently, more propagation and larger velocities. The influence of μ_c is more complex to interpret since $\mu_c = 0.6$ seems to be in the vicinity of a threshold value. For $\mu_c = 0.4$, the blocks propagate preferentially by sliding with small frictional dissipation and thus travel further than for $\mu_c = 0.6$. For $\mu_c = 0.8$, block tend to more preferentially roll and thus also propagate further than for $\mu_c = 0.6$.

4.3. Predictive capabilities of the block propagation model

The soil parameters calibrated in 2D using the experimental results on path A (Table 1) have been used in 2D simulations to predict block propagation on path B. The predictions obtained provide relevant information concerning the preferential deposit zones, the mean velocities at $ES1-B$ and the velocity range at $ES2-B$ (Fig. 13). However, the percentages of block stopped are underestimated for zone $1B$ and $3B$ and overestimated for zones $2B$ and $4B$. The extremely low and high values of velocities at $ES1-B$ are also not predicted. Finally, the details of velocity distribution at $ES2-B$ are not predicted. One can note that the variability of the results for different simulation sets is of the same order as for path A.

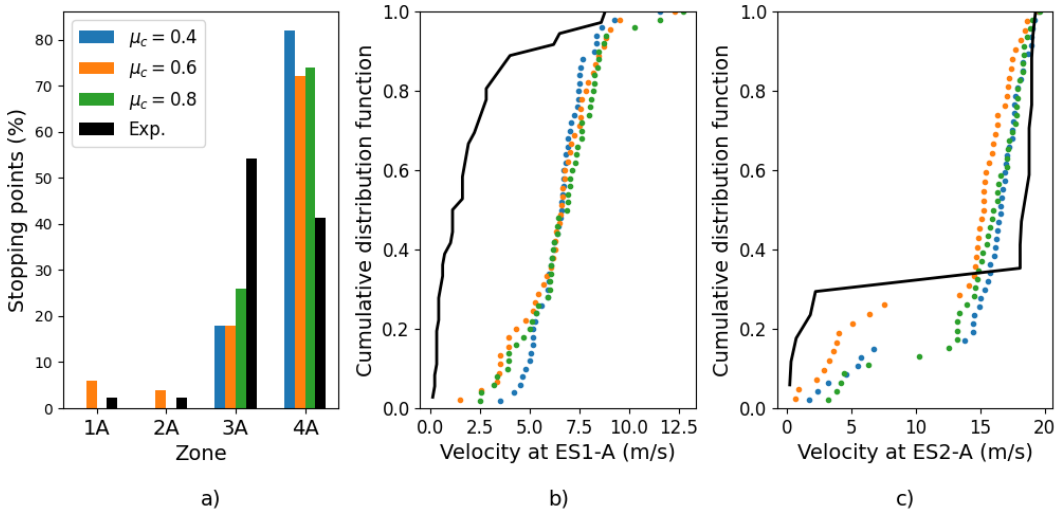

Figure 10.: Results obtained from different simulations of block propagation on path A using $e_c = 0$, $\mu_{r,c} = 0$ and different values of μ_c (a : distribution of the stopping points between the preferential deposit zones, b : cumulative distribution function of block velocities at $ES1 - A$, c : cumulative distribution function of block velocities at $ES2 - A$).

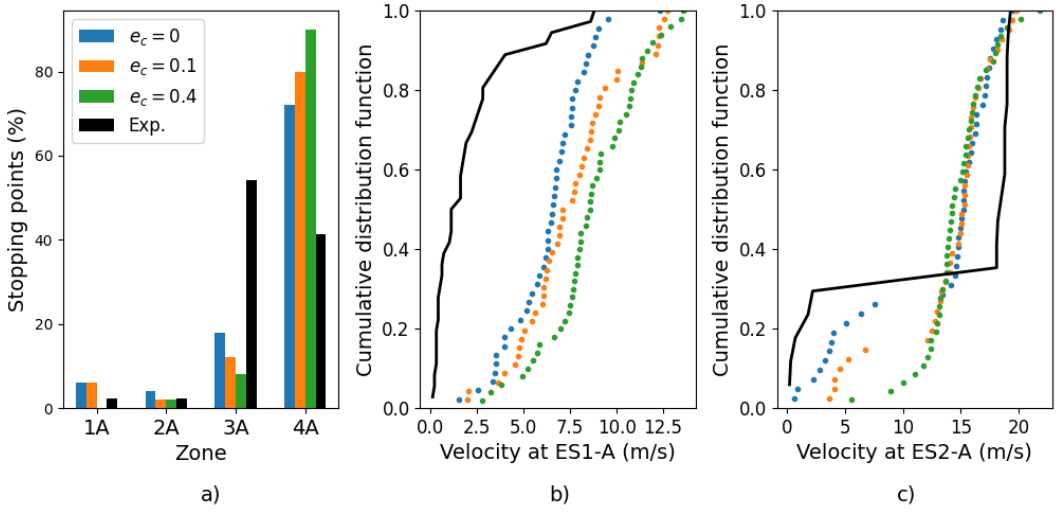

Figure 11.: Results obtained from different simulations of block propagation on path A using $\mu_c = 0.6$, $\mu_{r,c} = 0$ and different values of e_c (a : distribution of the stopping points between the preferential deposit zones, b : cumulative distribution function of block velocities at $ES1 - A$, c : cumulative distribution function of block velocities at $ES2 - A$).

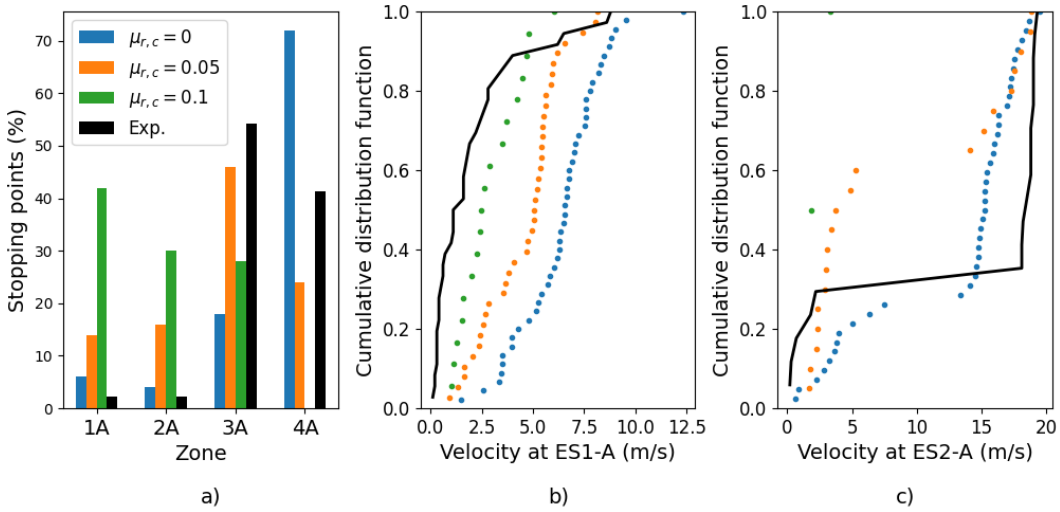

Figure 12.: Results obtained from different simulations of block propagation on path A using $e_c = 0$, $\mu_c = 0.6$ and different values of $\mu_{r,c}$ (a : distribution of the stopping points between the preferential deposit zones, b : cumulative distribution function of block velocities at $ES1 - A$, c : cumulative distribution function of block velocities at $ES2 - A$).

The use of 3D simulations to predict block propagation on path B using soil parameters calibrated in 2D on path A improves the quality of the predictions (Fig. 14) in terms of velocity distribution prediction and relative order of the preferential deposit zones. Quantitatively, the same differences as for 2D simulations are observed.

Interestingly, simulations of block propagation in 3D on path A (Fig. 15) using the same soil properties as in 2D provides slightly better results in terms of velocity distribution prediction. However, the limitation concerning the too numerous block stoppings in the uphill part of the site remains.

Finally, the distribution of the block stopping points obtained from 3D simulations (Fig. 16) on path A exhibit similar lateral dispersion as in the experiments. As observed in Fig. 15, a significantly too large amount of blocks is stopped in the uphill slope. For path B, although too many blocks are stopped on the uphill track compared to the ones stopped on the downhill one, the simulations predict well the substantial 3D deviations of the blocks from the main corridor.

5. Conclusion

The model proposed is based on a rigorous mechanical and numerical modelling of block propagation that focuses on the main parameters influencing the propagation. The model allows to integrate the effects of topography, block shape, initial location and orientation in a detailed manner and a contact model is integrated to traduce the interaction between the soil and block. The contact model, based on sound mechanical

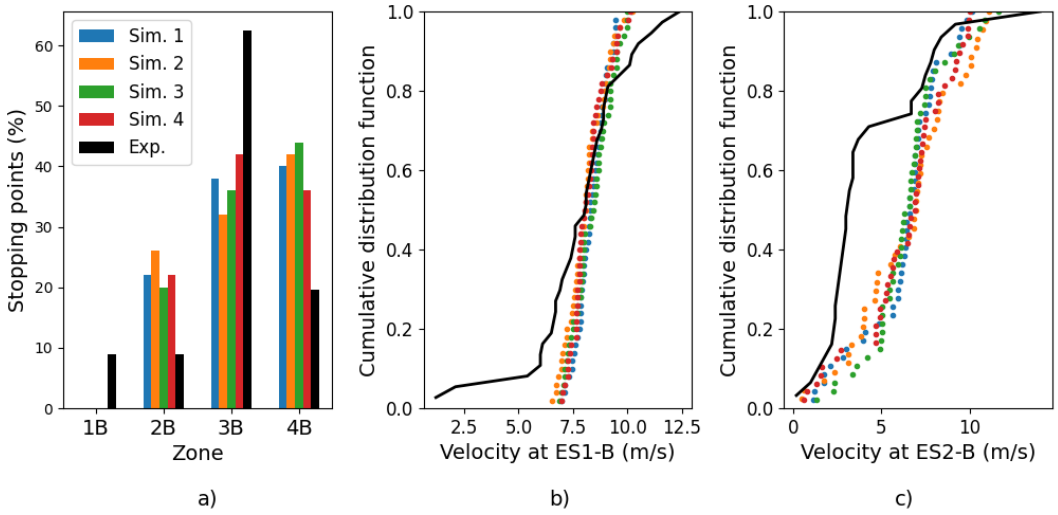

Figure 13.: Predictions of block propagation on path B obtained from 2D simulations with different simulation sets using the calibrated parameters for soil properties and $n = 50$ (a : distribution of the stopping points between the preferential deposit zones, b : cumulative distribution function of block velocities at $ES1 - B$, c : cumulative distribution function of block velocities at $ES2 - B$).

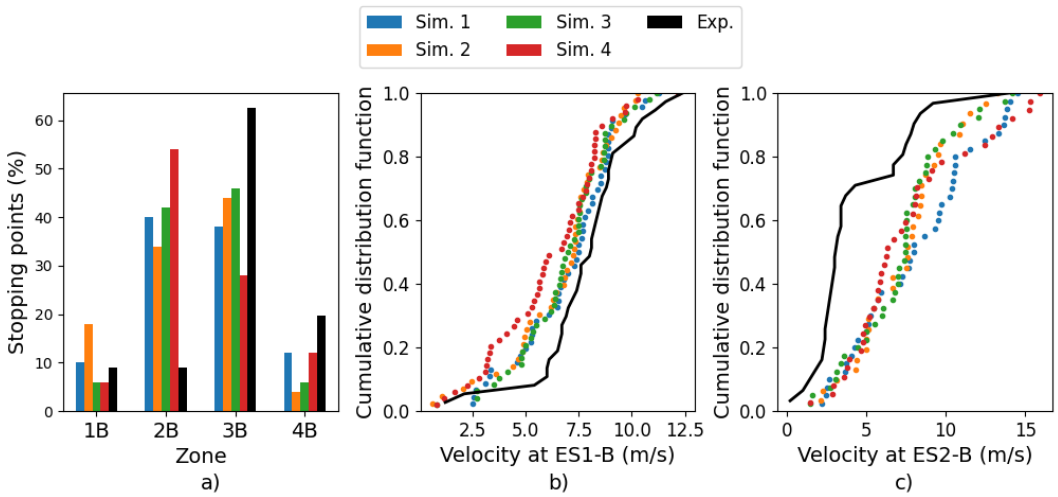

Figure 14.: Predictions of block propagation on path B obtained from 3D simulations with different simulation sets using the calibrated parameters for soil properties and $n = 50$ (a : distribution of the stopping points between the preferential deposit zones, b : cumulative distribution function of block velocities at $ES1 - B$, c : cumulative distribution function of block velocities at $ES2 - B$).

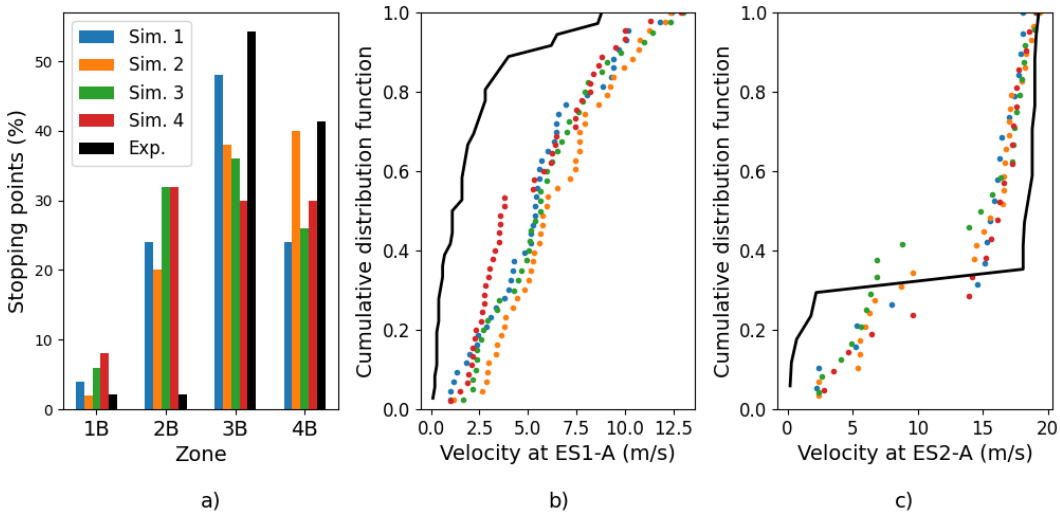

Figure 15.: Predictions of block propagation on path A obtained from 3D simulations with different simulation sets using the calibrated parameters for soil properties and $n = 50$ (a : distribution of the stopping points between the preferential deposit zones, b : cumulative distribution function of block velocities at $ES1 - A$, c : cumulative distribution function of block velocities at $ES2 - A$).

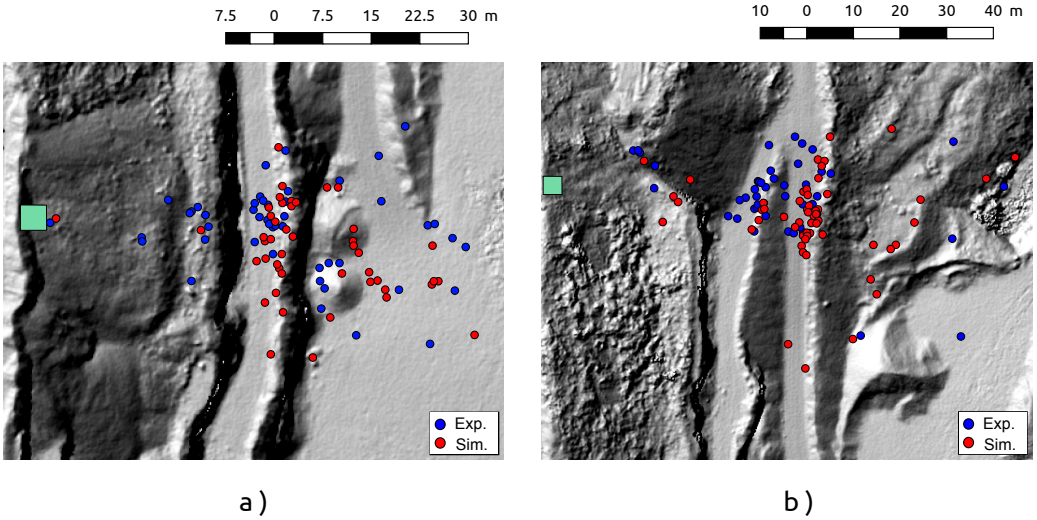

Figure 16.: Predictions of block stopping points on path A (a) and path B (b) obtained from 3D simulations with simulation sets using the calibrated parameters for soil properties and $n = 50$.

bases, involves a limited number of parameters related with the main physical process. The restitution coefficient quantifies soil plasticity, viscosity and mechanical waves propagation, the friction at the interface is also implemented as well as a rolling friction process which models cratering and resistance of the soil to block rolling around the contact point. In total, only three parameters are required to define soil properties in terms of interaction with the block.

The modelling approach proposed is among the more complex and detailed ones in trajectory analyses. The model belongs to the class of "rigid body" models which are classically identified as more complex than "lumped mass" ones (Volkwein et al., 2011). Compared to "lumped mass" models, "rigid body" models are based on more advanced mechanical concepts. In particular, instead of considering the block as a material point and using rebound models involving changes of the block velocities at its gravity centre only, they model explicitly the block shape and the interaction at the contact scale. This increased complexity does not necessarily entail increase in the number of parameters and simplifies the physical interpretation of the results. Among the propagation models explicitly integrating block shape, the model proposed is based on nonsmooth mechanics which allows a modelling of the contact as an interaction between perfectly rigid bodies. All the dissipation processes are modeled in the interface, keeping the intrinsic sticking feature of friction. In standard discrete element methods, Coulomb friction is generally regularized leading to non realistic viscous friction when sticking. This approach does not require introducing local compliance at the contact scale which is usually difficult to measure experimentally, does not introduce damping, and allows a more diversified use of numerical solving schemes. In particular, the numerical scheme used in this study allows to suppress unrealistic energy balance due to an artificial introduction of viscosity to ensure the numerical stability. The specificity of the modelling approach proposed will be crucial for several modelling improvements envisaged such as, for instance, the coupling with other mechanical models (e.g. models of protection structures) or the modelling of block fragmentation during propagation. One can note that most of the modelling features presented in this paper are freely available in the open-source block propagation models platform Platrock[2] and its coupling with Siconos.

In addition, both the simulation procedure and the calibration approach constitute original contributions of this work.

The principles of the simulation procedure favors practical use of the modelling approach. In particular, the variability of the parameters that cannot be estimated in the field (block shape and initial orientation, in this study) is explored statistically while the parameters that be can assessed in the field are explicitly set by the modeller. In the context of this study, the parameters set by the modeller were the global block properties (mass and sizes), the topography, and the release zone location, including the release height. The soil properties are also modeller-defined parameters but they

[2]https://gitlab.com/platrock/platrock

are more difficult to set since they cannot directly be measured. In this study, they were first calibrated and, second, used as input parameters to assess the predictive capabilities of the model.

A calibration procedure based on expert settings of the soil properties by trial and error was chosen in accordance with the engineering practices in the field of trajectory analysis. The fact that the calibration is based on 2D propagation models, favors its feasibility, given the computational efficiency of 2D models, and the experimental dataset used allows to separate calibration of the model and assessment of its predictive capabilities. Complementary, the use of calibration data at the field scale, of block stopping points locations in particular, favors the applicability of the procedure proposed since the latter data is more easily accessible to practitioners, compared to data at the rebound scale, in particular. Finally, this study presents a calibration based on comparisons to the complete distributions of several experimental measurements, and not only to global indicators (such as mean or maximum values) of these distributions, which not usual in the literature.

As classically in trajectory analyses, the calibrated model simulations predict the main characteristics of the propagation but not the quantitative details of the stopping points and velocities distributions. The simulations performed with the calibrated model on path B show the capacity of the model to predict the main characteristics of the propagation on path B both using 2D and 3D simulations. The level of adequacy between the experimental and simulation results is of the same order as in the calibration phase, i.e. for 2D simulations on path A. The similar level of adequacy between simulations and experimental results in the calibration and validation phases highlights that rebound model parameters can be associated with soil types, at least on this example. This generic feature of the model setting is crucial in terms of applicability since, after a calibration phase on sufficient amount of soil types, the model may be used in a predictive manner. The adequacy between 2D and 3D simulations is also an advantage in terms of applicability since 2D calibrations are substantially easier and faster than 3D ones.

Although the modelling of the field experiments provides a first overview of the use of the propagation model proposed, the modelling approach has to be adapted for a practical use since the conditions of the field experiments presented do not fully correspond to typical practical conditions. In particular, in practice, the block release point, volume, shape and orientation are not fixed. They have to be assessed from field observations and, in most cases, release point locations and volumes have to be explored statistically in addition to block shape and orientation. In addition, in the absence of an exhaustive calibration of the model for a large range of soil types, additional calibrations have to be done which is a difficult task mainly because of the questions of the amount and of the type of data required for a correct calibration.

The results presented in this paper exhibit a level of adequacy that may not look sufficient for a quantitative design of protection structures or for precise hazard zona-

tion. However, the results tend to show that the adequacy lacks are more in the details of the velocity distribution than in the global range of velocities. Consequently, it may be possible to design a structure on the basis of the predicted extreme quantities. In the same vein, differences in terms of block stopping points are mainly observed for small and median propagation distances which is of smaller importance in practice. In addition, the level of adequacy, although rather small, can be completed with uncertainties assessment to provide additional information that will increase awareness in the process of design or zonation. Finally, a promising perspective for the improvement of model adequacy is the design of more advanced calibration procedures based on the optimization of the parameters values.

References

Acary, V. (2015). Energy conservation and dissipation properties of time-integration methods for the nonsmooth elastodynamics with contact. Article published online.

Acary, V., Bonnefon, O., Brémond, M., Huber, O., Pérignon, F., and Sinclair, S. (2019). An introduction to Siconos. Technical Report RT-0340, INRIA.

Acary, V. and Bourrier, F. (2021). Coulomb friction with rolling resistance as a cone complementarity problem. European Journal of Mechanics, A/Solids, 85.

Acary, V., Brémond, M., and Huber, O. (2018). Advanced Topics in Nonsmooth Dynamics., chapter On solving frictional contact problems: formulations and comparisons of numerical methods. Acary, V. and Brüls. O. and Leine, R. (eds). Springer Verlag.

Acary, V. and Brogliato, B. (2008). Numerical methods for nonsmooth dynamical systems. Applications in mechanic Lecture Notes in Applied and Computational Mechanics 35. Berlin: Springer. xxi, 525 p. .

Asteriou, P. and Tsiambaos, G. (2018). Effect of impact velocity, block mass and hardness on the coefficients of restitution for rockfall analysis. International Journal of Rock Mechanics and Mining Sciences, 106:41 – 50.

Bourrier, F., Berger, F., Tardif, P., Dorren, L., and Hungr, O. (2012). Rockfall rebound: comparison of detailed field experiments and alternative modelling approaches. Earth Surface Processes and Landforms, 37(6):656–665.

Bourrier, F. and Hungr, O. (2013). Rockfall Engineering, chapter Rockfall Dynamics: A Critical Review of Collision and Rebound Models, pages 175–209. ISTE-Wiley.

Bourrier, F., Toe, D., Garcia, B., Baroth, J., and Lambert, S. (2020). Experimental investigations on complex block propagation for the assessment of propagation models quality. Landslides.

Brogliato, B. (2016). Nonsmooth Mechanics: Models, Dynamics and Control. Communications and Control Engineering. Springer-Verlag, London, 3nd edition.

Caviezel, A., Demmel, S. E., Ringenbach, A., Bühler, Y., Lu, G., Christen, M., Dinneen, C. E., Eberhard, L. A., von Rickenbach, D., and Bartelt, P. (2019). Reconstruction of four-dimensional rockfall trajectories using remote sensing and rock-based accelerometers and gyroscopes. Earth Surface Dynamics, 7(1):199–210.

Crosta, G. and Agliardi, F. (2004). Parametric evaluation of 3D dispersion of rockfall trajectories. Natural Hazards and Earth System Sciences, 4:583–598.

Descoeudres, F. and Zimmermann, T. (1987). Three-dimensional dynamic calculation of rockfalls. In Proceedings of the 6th International Congress on Rock Mechanics - Montreal, pages 337–342, Rotterdam. Balkema.

Dorren, L. (2003). A review of rockfall mechanics and modelling approaches. Progress in Physical Geography, 27(1):69–87.

Dorren, L., Berger, F., and Putters, U. (2006). Real-size experiments and 3D simulation of rockfall on forested and non-forested slopes. Natural Hazards and Earth System Sciences, 6(1):145–153.

EOTA (2018). Falling rock protections kits. ead 340059-00-0106/c 417/07. technical report.

Falcetta, J.L. (1985). Un nouveau modèle de calcul de trajectoires de blocs rocheux. Rev. Fr. Geotech., (30):11–17.

Garcia, B., Richefeu, V., Baroth, J., Daudon, D., and Villard, P. (2020). Collision of shaped boulders with sand substrate investigated by experimental, stochastic, and discrete approaches. Journal of Geophysical Research: Earth Surface, 125(11).

Géradin, M. and Cardona, A. (2001). Flexible Multibody Dynamics: A finite element Approach. J. Wiley & Sons, New York. 340 p.

Giani, G. P., Giacomini, A., Migliazza, M., and Segalini, A. (2004). Experimental and theoretical studies to improve rock fall analysis and protection work design. Rock Mechanics and Rock Engineering, 37(5):369–389.

Guzzetti, F., Crosta, G., Detti, R., and Agliardi, F. (2002). Stone: a computer program for the three-dimensional simulation of rock-falls. Computer and Geosciences, 28:1079–1093.

Hu, J., Li, S., Li, L., Shi, S., Zhou, Z., Liu, H., and He, P. (2017). Field, experimental, and numerical investigation of a rockfall above a tunnel portal in southwestern china. Bulletin of Engineering Geology and the Environment.

Jean, M. and Moreau, J. (1987). Dynamics in the presence of unilateral contacts and dry friction: a numerical approach. In Del Pietro, G. and Maceri, F., editors, Unilateral problems in structural analysis. II, pages 151–196. CISM 304, Spinger Verlag.

Jourdan, F., Alart, P., and Jean, M. (1998). A Gauss Seidel like algorithm to solve frictional contact problems. Computer Methods in Applied Mechanics and Engineering, 155(1):31–47.

Koo, C. and Chern, J. (1998). Modification of the dda method for rigid block problems. International Journal of Rock Mechanics and Mining Sciences, 35(6):683–693.

Labiouse, V. and Heidenreich, B. (2009). Half-scale experimental study of rockfall impacts on sandy slopes. Natural Hazards and Earth System Sciences, 9(6):1981–1993.

Lan, H., Derek Martin, C., and Lim, C. (2007). Rockfall analyst: A GIS extension for three-dimensional and spatially distributed rockfall hazard modeling. Computers and Geosciences, 33(2):262–279.

Leine, R. I., Schweizer, A., Christen, M., Glover, J., Bartelt, P., and Gerber, W. (2014). Simulation of rockfall trajectories with consideration of rock shape. Multibody System Dynamics, 32(2):241–271.

Lu, G., Caviezel, A., Christen, M., Demmel, S., Ringenbach, A., Bühler, Y., Dinneen, C., Gerber, W., and Bartelt, P. (2019). Modelling rockfall impact with scarring in compactable soils. Landslides, 16(12):2353–2367.

Lu, G., Ringenbach, A., Caviezel, A., Sanchez, M., Christen, M., and Bartelt, P. (2020). Mitigation effects of trees on rockfall hazards: does rock shape matter? Landslides.

Mollon, G., Richefeu, V., Villard, P., and Daudon, D. (2012). Numerical simulation of rock avalanches: Influence of a local dissipative contact model on the collective behavior of granular flows. Journal of Geophysical Research: Earth Surface, 117(2). cited By 30.

Moreau, J. (1988). Unilateral contact and dry friction in finite freedom dynamics. In Moreau, J. and P.D., P., editors, Nonsmooth Mechanics and Applications, pages 1–82. CISM 302, Spinger Verlag. Formulation mathematiques tire du livre Contacts mechanics.

Spadari, M., Giacomini, A., Buzzi, O., Fityus, S., and Giani, G. (2012). In situ rockfall testing in new south wales, australia. International Journal of Rock Mechanics and Mining Sciences, 49:84 – 93.

Toe, D., Bourrier, F., Dorren, L., and Berger, F. (2018). A novel dem approach to simulate block propagation on forested slopes. Rock Mechanics and Rock Engineering, 51(3):811–825.

Volkwein, A., Brügger, L., Gees, F., Gerber, W., Krummenacher, B., Kummer, P., Lardon, J., and Sutter, T. (2018). Repetitive rockfall trajectory testing. Geosciences (Switzerland), 8(3).

Volkwein, A., Schellenberg, K., Labiouse, V., Agliardi, F., Berger, F., Bourrier, F., Dorren, L., Gerber, W., and Jaboyedoff, M. (2011). Rockfall characterisation and structural protection - a review. Natural Hazards and Earth System Science, 11(9):2617–2651.

Williams, C., Morkeh, J., Dorfschmidt, K., Poon, C., Matlashewski, P., and Carvalho, J. (2020). Innovative rockfall solutions based on calibration and field testing. Mining, Metallurgy and Exploration, 37(1):101–116.

Yan, P., Zhang, J., Kong, X., and Fang, Q. (2020). Numerical simulation of rockfall trajectory with consideration of arbitrary shapes of falling rocks and terrain. Computers and Geotechnics, 122.